



UvA-DARE (Digital Academic Repository)

Use of prior knowledge in biological systems modelling

Reshetova, P.V.

Publication date

2017

Document Version

Other version

License

Other

[Link to publication](#)

Citation for published version (APA):

Reshetova, P. V. (2017). *Use of prior knowledge in biological systems modelling*. [Thesis, fully internal, Universiteit van Amsterdam].

General rights

It is not permitted to download or to forward/distribute the text or part of it without the consent of the author(s) and/or copyright holder(s), other than for strictly personal, individual use, unless the work is under an open content license (like Creative Commons).

Disclaimer/Complaints regulations

If you believe that digital publication of certain material infringes any of your rights or (privacy) interests, please let the Library know, stating your reasons. In case of a legitimate complaint, the Library will make the material inaccessible and/or remove it from the website. Please Ask the Library: <https://uba.uva.nl/en/contact>, or a letter to: Library of the University of Amsterdam, Secretariat, Singel 425, 1012 WP Amsterdam, The Netherlands. You will be contacted as soon as possible.

Chapter 4

Computational model reveals limited correlation between germinal centre B-cell subclone abundancy and affinity: implications for repertoire sequencing³

Immunoglobulin repertoire sequencing strategies are successfully applied to identify expanded antigen-activated B-cell clones that play a role in the pathogenesis of immune disorders. These clones comprise lineages of subclones comprising variants within a VJ family produced by somatic hypermutation. Their B-cell receptor binding affinities for the antigen are higher than affinities of the naïve B cells in the background population, which is a direct consequence of the higher initial affinity of the activated B-cell(s) and the subsequent affinity maturation process in the germinal centre (GC). However, repertoire sequencing only provides information about subclone abundancies and not about their affinities. Consequently, although repertoire sequencing successfully identifies (sub)clones involved in disease, the selection of the most abundant (i.e., expanded) subclone(s) within of a clonal family may not necessarily be the highest affinity subclone. Unfortunately, the determination of affinities of many subclones within a clonal family is virtually impossible and, consequently, the relation between abundancy and affinity remains to be established. Knowledge about affinities within clonal families would likely improve the selection of relevant subclones for further characterization and antigen screening. Therefore, to gain insight in the putative affinity distribution among (un)expanded subclones we developed a computational model that simulates affinity maturation in a single GC while tracking individual subclones in terms of abundancy and affinity. We show that the model correctly captures the overall GC dynamics, and that the amount of expansion is qualitatively comparable to expansion observed from B cells isolated from a normal human lymph node. Analysis of the fraction of high- and low-affinity subclones among of the unexpanded and expanded subclones reveals a only partial correlation between abundancy and affinity and that the low abundant subclones are of highest affinity. Thus, our

³P. Reshetova, B.D.C. van Schaik, P.L. Klarenbeek, M.E. Doorenspleet, R.E.E. Esveldt, P.P. Tak, J.E.J. Guikema, N. de Vries, A.H.C. van Kampen. Manuscript in preparation.

model suggests that selecting highly abundant subclones from repertoire sequencing does not automatically provides us the highest affinity B cell. We conclude that although selection of highly abundant subclones from B cell repertoires provides us with B cells involved in (auto)immune disorders, the utility of repertoire sequencing might be even further improved by following selection strategies that do not merely consider subclone abundance.

4.1. Introduction

The adaptive immune system is a key component of our defense against pathogens and comprises highly specialized cells and processes. Its humoral component is responsible for memory B-cell formation and high-affinity antibody (Ab) production resulting from affinity maturation in germinal centers (GCs) [91, 92]. During this process GC B cells undergo multiple rounds of proliferation, somatic hypermutation (SHM), and selection to improve their affinity for the given antigen (Ag). This results in a dynamic ensemble of low and high affinity B-cell subclones comprising variants of a clone within a VJ family produced by SHM. Higher affinity cells have increased chance to be positively selected for further rounds of proliferation and SHM, or for differentiation to memory and plasma cells.

Repertoire sequencing using high-throughput sequencing enables the determination of T- and B-cell repertoires in (clinical) samples by sequencing the expressed V, D, and J gene segments [93, 94, 95, 96]. Immune responses typically involve the initiation and coexistence of up to several hundreds of GCs, which emerge over an extended period of time [97, 98, 99]. Consequently, B-cell repertoire sequencing of clinical samples typically identifies (sub)clones originating from a multitude of Ag-activated B cells and GCs, or even from responses to multiple Ags. Despite this complexity we and others successfully used repertoire sequencing for the identification of (autoreactive) B cells involved in immune disorders while relying on the assumption that expanded clones play a key role in the pathogenesis of the disease [100, 101]. An expanded clone comprises a B-cell lineage of related subclones varying in abundance and number of acquired somatic mutations. B-cell receptor binding affinities for the antigen of these subclones are expected to be higher than affinities of the naive B cells in the background population, which is a direct consequence of the higher initial affinity for the Ag of the activated B-cell(s) and the subsequent affinity maturation process. However, repertoire sequencing only provides information about subclone abundancies and not about their affinities. Consequently, although repertoire sequencing successfully identifies clones involved in disease, the selection of the most abundant (i.e., expanded) subclone(s) within a clonal family may not correspond to the highest affinity subclone. Unfortunately, the determination of affinities of the many subclones within a clonal family is virtually impossible with current experimental technologies. Since cells are destructed in the sequencing experiment, affinity analysis requires either labor-intensive selective cloning of the individual B cells, or equally labor-intensive expression of single BCRs in cloning systems. Currently, these requirements prohibit high-throughput analysis of affinity of sequenced cells. Moreover, measurement of affinities also require knowledge of the Ag which is often not available for clinical samples. Only part of the subclones within a clonal lineage reaches high cell counts and these are typically selected for further characterization and Ag screening [100]. Given the nature of affinity maturation one would expect that high

abundant subclones are of highest affinity, which would argue for the selection of the most abundant subclone as a viable strategy. However, since the relation between abundance and affinity is unknown, it cannot be excluded that a fraction of the large subclones are of low affinity and *vice versa*. Therefore, alternative (affinity-based) selection strategies might be of added value for downstream analysis.

In this work we developed a computational model of a single GC to gain insight in the putative affinity distribution among expanded and unexpanded subclones identified by B-cell repertoire sequencing. Inspired by existing models of affinity maturation (e.g., [102, 103, 104, 105]), we implemented a mathematical model that comprises a large evolving set of ordinary differential equations (ODEs) providing information about the abundance and affinity of individual subclones emerging during the GCR. We did not use one of the existing models since existing ODE models do not track individual subclones while agent based models (e.g., [105]) are faced with the additional complexity of GC spatial dynamics which we aimed to avoid. Moreover, most models are not available as a software implementation.

We show that our computational model is in agreement with the typical GC dynamics. We also show that the amount of expansion of selected B-cell lineages from repertoire data acquired from a human lymph node is qualitatively comparable to the level of expansion observed in the simulated data. Given this support for our model, we subsequently inspected the affinities and abundancies of the individual subclones from the simulations, and found that the expanded and unexpanded B-cell subclone compartments each comprise a mixture of high and low affinity cells, i.e., there is only partial correlation between affinity and abundance of subclones within a clonal family. Moreover, the low abundant subclones were of highest affinity. Consequently, although repertoire sequencing enables the correct identification of expanded clones involved in immune disorders, the subsequent selection of high-abundant subclones within a clonal family does not necessarily result in the highest affinity subclone. Although at this stage these results cannot be experimentally validated, we argue that considering only subclone abundance might not be the most optimal strategy to select candidate B-cell clones for further characterization and Ag screening.

4.2. Material and Methods

Sample and experimental data

We selected a single sample for analysis and comparison to the simulation results. This sample represents leukocytes isolated from a lymph node from an otherwise healthy human individual, without ongoing infection (represented in biochemical parameters such as C-reactive protein). The sample was taken as described earlier [106]. Repertoire sequencing was performed as described in [93] using the Roche 454 sequencing platform to generate 7771 reads (6777 unique reads). Processing of the sequence data was performed as described in [93]. In brief, reads from a multiplexed sequence run were separated by their multiplex identifiers (MID) and aligned against the IMGT database [107] with BLAT [108] to identify the corresponding V and J segments. Subsequently, each read was translated to a peptide sequence and the CDR3 sequence was determined by identifying conserved motifs in the V and J segment that delineate the CDR3 [109]. Conse-

quently, only in-frame reads were used. Sequences with uncalled bases in their CDR3 region were excluded from analysis. This resulted in 4454 unique subclones (clones within a VJ family defined as a peptide with a unique V and J assignment, and unique CDR3 sequence). This amount of sequence reads is sufficient to represent capture most (expanded) subclones but may miss subclones occurring at very low frequencies. A full analysis and presentation of this and other lymph node samples we have will be part of future paper.

The mathematical model

We developed a mathematical model using ordinary differential equations (ODEs) to describe the dynamics of individual subclones during the GCR. This model is implemented in the R statistical environment version 3.2.2 [110] using R packages `deSolve` (version 1.12) [111], `R6` (version 2.1.2), `ggplot2` 2.0 and `beeswarm` 0.2.1. The software is available as open source (GPLv3) on request from the author.

Overall simulation setup

Our simulation framework represents a simplified but adequate model of the GCR [92, 91] (Figure 4.1). Briefly, prior to the GCR, B cells and T cells are activated by recognition of their cognate antigen in the primary follicle and T-cell zone respectively (day -2 in Figure 4.1). Activated B cells and T cells migrate to the interfollicular region and interact resulting in the full activation of B cells while the T cells differentiate to T follicular helper cells (Tfh). Two days after immunization the GCR is initiated (day 0 in our simulation) with the Tfh cells and activated B cells migrating into the follicle, which is characterized by a network of follicular dendritic cells (FDCs). Here, the B cells engage in a rapid monoclonal expansion to over 10,000 cells at day 4 forming the GC. During this expansion a dark zone comprising centroblasts (CBs) and a light zone comprising centrocytes (CC), FDCs and Tfh cells are established. The dark zone is the site of B-cell clonal expansion and BCR diversification through SHM producing novel subclones. The GC light zone is the site of positive B-cell selection through Ag and Tfh binding and signaling. Together, these processes are responsible for B-cell affinity maturation. SHM has been reported to start at day 7 post-immunization in mice [112]. Oprea and Perelson [102] assumed that the GC is initiated 3 days after immunization and, correspondingly, start SHM at day 4 of the GCR in their model. Others reported that SHM starts 2 days post-immunization [113], or even prior to GC formation [114]. Following Oprea and Perelson, we also start SHM at day 4 in our simulations. Following monoclonal expansion, memory cells and plasma cells are starting to be produced (day 4 in our simulation). Although the precise mechanisms and timing of the output cells are not well-understood [115], it has been proposed that initially mainly memory B cells are produced while at later stages the GCR is dedicated towards (higher affinity) long-lived plasma cells [116, 117]. In our model the production of memory and plasma cells starts at the same moment (day 4) but we made the rate of plasma cell differentiation dependent on the absolute affinity of the CCs resulting in a low plasma cell output during early stages of the GCR. Since we were not interested in the production of output cells, these are not further discussed in this paper. Our simulation starts at day 0 with three founder B cells (CBs) with different affinities, and terminates after 21 days, the life span of an average GC. Consequently, we

do not model GC shutdown since its mechanisms remain to be established. Our model does not explicitly include the dark/light zones, Ags, FDCs, or Tfh cells since we are not interested in the spatial dynamics nor in the precise selection mechanisms but rather in modelling subclonal diversity, expansion, and affinity. Therefore, to avoid an overly complex model, we represent the Ag and Tfh survival signals with sigmoidal functions as explained below.

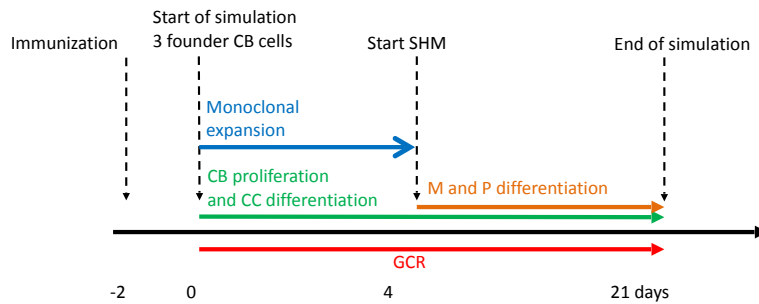


Figure 4.1: Simulation time line of the germinal center reaction. The GCR starts with 3 founder B cells (affinities 0.1, 0.2 and 0.3 μM) 2 days after immunization and continues for 21 days.

Somatic hypermutation, subclones, and affinity

The V, D, and J segments that make up the BCR cover four framework regions (FWRs) providing the Ab structural framework, and three Ag-binding complementary determining regions (CDRs) [118, 119]. Our model considers the FWR and CDR regions without an explicit nucleotide representation of the BCR but, instead, using a decision tree that decides on the fate of each individual SHM [103, 120, 121] (Figure 4.2). This tree involves probabilities for silent (synonymous mutations), lethal FWR, and affinity changing CDR mutations. The probabilities for replacement and silent mutations were determined from many mice germline sequences. The probability of the lethal mutations was based on studies that analyzed mutations patterns in real sequences. To determine the number of mutations during each CB cell division we defined the BCR to have a length of 600 nucleotides (i.e., one light and heavy chain). Given that the SHM rate is 10^{-3} per bp per division which this results in 0.6 mutations per division. We model this as a Poisson distribution $m = Poisson(\lambda = 0.6)$ and, consequently, each cell acquires 0, 1, or more mutations after each cell division. The mutation decision tree distinguishes the CDRs and their surrounding structural FWRs but does not differentiate between CDR1, CDR2 and CDR3 [119, 118].

In repertoire sequencing one is usually interested determining the population of (sub)clones in an immune response. Each of these subclones has its own binding affinity for the Ag. Since the CDR3 region is the main determinant in Ag-binding, one generally defines and discriminates these subclones on the basis of their unique CDR3 peptide sequence (within a VJ family). Alternatively, we can also define a subclone as having a unique BCR nucleotide sequences (i.e., V-CDR3-J). In the first situation, only non-synonymous SHMs in the CDR3 region produce new subclones, while in the second

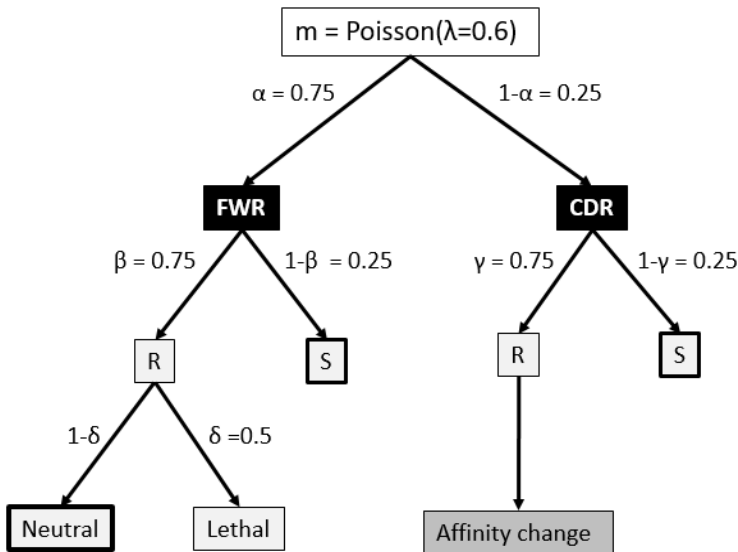


Figure 4.2: Fate of each somatic hypermutation. After each CB division the daughter cells are affected by $m \geq 0$ mutations affecting the framework region (FWR) with a probability of α or the complementary determining region (CDR). A mutation may replace (R) an amino acid of the Ig FWR or CDR region with probability β and γ respectively. A mutation in the FWR is lethal with probability δ . A replacement mutation in the CDR is neutral or changes the affinity of the subclone. Part of our simulations neglect mutations indicated by the thick boxes to produce subclones at the peptide level. Probabilities in this tree are according to [103].

situation each non-lethal SHM results in a new subclone. The mutation decision tree (Figure 4.2) is defined at the level of the nucleotide sequence and, consequently, in our simulation we implicitly define and track subclones at the nucleotide level throughout the GCR. Consequently, each SHM generates a new subclone that is initially represented as a single CB that subsequently proliferates and differentiates to co-exist as CB, CC, memory cell and plasma cell at succeeding time points. Alternatively, we may consider only CDR replacement mutations to define and track subclones at the peptide level. In this situation, each non-lethal replacement mutation in the CDR generates a new subclone. Since the tree does not specifically distinguish CDR3 from CDR1 and CDR2, our simulations at the peptide level effectively includes all three CDRs, which may give an overestimation of the number of unique clones compared to only considering the CDR3 as is done in repertoire sequencing experiments. However, since all three CDR regions are involved in Ag binding the simulation might be more realistic. Subclones with CB cell counts less than one (a result from using continuous differential equations; see below) are kept in our simulation but are not further be affected by SHM to avoid the generation of new subclones from these cells.

Each subclone in our model has a unique BCR with an absolute affinity σ that specifies the interaction strength with the Ag. The affinities of the three single cell founder CBs are set to arbitrary but different low affinity values (0.1, 0.3, and 0.5 μM). Three dif-

ferent values were chosen to establish an initial level competition between the founder cells. The magnitude of the initial affinities does not affect the dynamics of our model since this depends on relative affinities (see below). Only plasma cell output depends on absolute affinities. For each affinity changing mutation (Figure 4.2) the affinity of the affected subclone is updated according to $\sigma_{new\ subclone} = \sigma_{parent} + \Delta\sigma$ where $\Delta\sigma$ is drawn from a distribution $f(\sigma)$ with probability density function:

$$f(\sigma) = g(s, r) - \mu - (\sigma_{parent} * 0.1), \quad (4.1)$$

where $g(s, r)$ is the inverse gamma distribution with $s = 3$ and $r = 0.3$ representing the shape and rate parameter respectively. μ is the expected value of $g(s, r)$ and subtracted from $g(s, r)$ to center the distribution g around zero resulting in about equal chances for decreasing and increasing the affinity of mutated subclones. We used the gamma distribution because it is right skewed and, therefore, allows for a small chance for making larger affinity improvements representing key mutations [120, 122]. We do not distinguish between one or multiple affinity changing mutations. To account for the fact that mutations in higher affinity subclones have less chance to further improve affinity we shift distribution f to the left as a function of the parent cell affinity (Supplementary Figure S1). The distribution shape and rate parameters (3 and 0.3) and the affinity shift (0.1) were chosen by trial and error such to obtain the dynamics of a typical GC.

Positive and negative selection of subclones

Following cell division and SHM, the CBs differentiate to CCs which are programmed to undergo apoptosis (negative selection) unless they receive survival signals (positive selection) through interactions with the Ag (presented by FDCs) and Tfh cells [91]. These selection mechanisms impose competition between the B-cell subclones, which is assumed to be based on their relative BCR affinities σ_{rel} [91]. CCs bind Ag to acquire their first survival signal. Subsequently, the Ag is internalized and presented to Tfh cells. Higher-affinity B cells present more Ag and, therefore, compete favorably for the limited number of Tfh cells to acquire a second survival signal. Positively selected may CCs recycle to the dark zone for further rounds of division and SHM, or they differentiate into memory cells or plasma B cells.

To avoid an overly complex model, Ag and Tfh survival signals are modelled with a sigmoidal function:

$$S(\sigma_{rel,i}) = \frac{\sigma_{rel,i}^n}{k^n + \sigma_{rel,i}^n}, \quad (4.2)$$

where i denotes a subclone. This function converts relative affinities $\sigma_{rel,i}$ to a signal strength between 0 and 1. Relative affinities are obtained by scaling absolute affinities σ to values between 0 and 1. Signal S affects the CB to CC differentiation rate ($\eta_{CB \rightarrow CC}$) and the CC apoptosis rate (μ_{CC}) (Equations 5.2a and 5.2b). Recently, it was shown that higher affinity cells stay longer in the dark zone further facilitating their expansion and diversification resulting in less apoptosis [123]. This is accommodated by our model by multiplying the CB to CC differentiation rate with $(1 - S)$ resulting in a rate between 0 and its maximum value $\eta_{CB \rightarrow CC}$ (Table 5.1). Similarly, a higher signal reduces the apoptosis

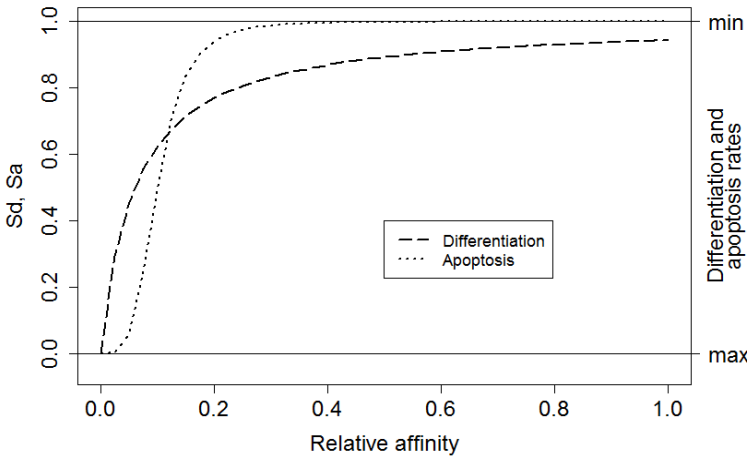


Figure 4.3: The relative affinity of each subclone determines the magnitude of the overall survival signal. Left axis: S_d corresponds to signal affecting the CB to CC differentiation rate (dashed line). S_a corresponds to the signal affecting CC apoptosis (dotted line). Right axis: effect of signal S on the differentiation and apoptosis rates. A high signal results in low differentiation and apoptosis rates.

rate. We assume that S does not affect these rates to the same extent and therefore we parameterized S differently for differentiation and apoptosis. We set $k = 0.06$ and $n = 1$ for differentiation (S_d), and $k = 0.1$ and $n = 4$ for apoptosis (S_a ; Figure 4.3). The parameters k and n were chosen to obtain a typical GC response that attains a maximum number of cells during the first phase of the GCR. During our simulation the emergence of new subclones with higher absolute affinity will “push” existing subclones with lower affinities to lower relative affinities as result of the scaling and, hence, to smaller survival signals resulting the vanishing of these subclones.

Ordinary differential equations

Each subclone i assumes 4 phenotypes: centrocytes (CC_i), centroblasts (CB_i), memory cells (M_i), and plasma cells (P_i) (Figure 4.4). The temporal dynamics of each individual subclone is described by a set of ordinary differential equations (ODEs) representing these four phenotypes (Equations 5.2a to 5.2d).

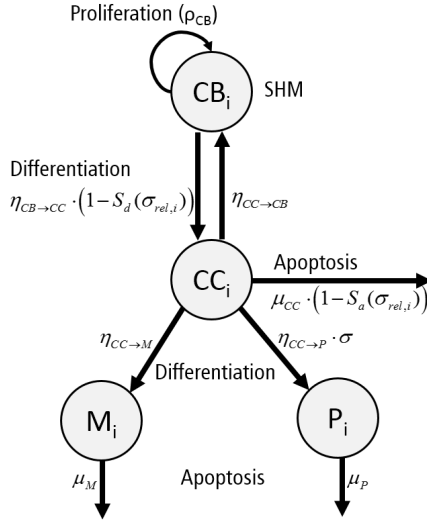


Figure 4.4: Graphical representation of the ordinary differential equations representing a single subclone i . Each subclone assumes four phenotypes: centrocytes (CC), centroblasts (CB), plasma cells (P) and memory cells (M). Cells proliferate (ρ_{CB}), differentiate ($\eta_{CB \rightarrow CC}, \eta_{CC \rightarrow CB}, \eta_{CC \rightarrow P}, \eta_{CC \rightarrow M}$), or go into apoptosis (μ_{CC}, μ_P, μ_M) with indicated rates. The apoptosis rate of CCs and differentiation rate of CBs depend on signal S_a and S_d respectively. Differentiation to plasma cells depend on the absolute affinity of the CCs.

$$\begin{aligned} \frac{dCB_i}{dt} = & \rho_{CB} \cdot \left(\frac{A^h}{CB_{total}^h + A^h} \right) \cdot CB_i + \eta_{CC \rightarrow CB} \cdot CC_i \\ & - \left(1 - S_d(\sigma_{rel,i}) \right) \cdot \eta_{CB \rightarrow CC} \cdot CB_i \end{aligned} \quad (4.3a)$$

$$\begin{aligned} \frac{dCC_i}{dt} = & \left(1 - S_d(\sigma_{rel,i}) \right) \cdot \eta_{CB \rightarrow CC} \cdot CB_i - \eta_{CC \rightarrow CB} \cdot CC_i \\ & - \left(1 - S_a(\sigma_{rel,i}) \right) \cdot \mu_{CC} \cdot CC_i - \eta_{CC \rightarrow M} \cdot CC_i \\ & - \eta_{CC \rightarrow P} \cdot \sigma_i \cdot CC_i \end{aligned} \quad (4.3b)$$

$$\frac{dM_i}{dt} = \eta_{CC \rightarrow M} \cdot CC_i - \mu_M \cdot M_i \quad (4.3c)$$

$$\frac{dP_i}{dt} = \eta_{CC \rightarrow P} \cdot \sigma_i \cdot CC_i - \mu_P \cdot P_i \quad (4.3d)$$

To allow the GC to grow to a sufficient number of cells during monoclonal expansion the signal $S_{\{d,a\}}$ is set to 0.9 for the first 4 days of the simulation to minimize differentiation of CBs to CCs and apoptosis of the initial CCs. The CB equation includes a density dependent expansion term defining nonspecific resource competition between the B cells, reducing their proliferation rate if the number of cells approaches A . The CC apoptosis rate and the CB to CC differentiation rate are multiplied by $(1 - S_{\{d,a\}}(\sigma_{rel,i}))$ for reasons explained above. Plasma cell differentiation depends on the absolute affinity σ_i

to reduce their production at earlier stages of the GCR. During the simulation we calculate the differential equations for periods of six hours (the duration of one CB division). After each period we impose SHM and update the population of subclones as described above. For each non-lethal SHM a new subclone and an additional set of four ODEs is created. The CB cell count for new subclones is set to one, while the corresponding cell counts for the CCs, memory cells and plasma B cells are set to zero. The CB cell count of the parent subclone is reduced by one. If the sum of CC and CB counts for subclone i is less than 0.1 cells we remove the subclone and corresponding equations from the system. Since SHM is a stochastic process that affects the subclone population and their (relative) affinities, we repeated simulations 15 times with the same initial conditions (three founder B cells with initial affinities 0.1, 0.3, and 0.5).

Model parameters

Parameter values for proliferation, differentiation, and apoptosis were obtained from literature (Table 5.1). Parameters A and h were chosen to limit the maximum size of the GC. Values for parameters for k , n , s , r , and affinity shift were straightforwardly acquired by trial-and-error aiming to produce a typical GC response with a peak of at least 10,000 cells during the first phase of the GCR with our model. There is very limited (quantitative) data describing the GC response. We are not aware of any data obtained from human samples describing the dynamics of GC volume (number of cells) during the GCR. Consequently, the precise timing and magnitude of the maximum GC response, its decay, the biological variation of this response across samples and organisms, and the factors affecting this this response remain to be established. The canonical GC response has, for example, been observed by tracking follicle center volume as fraction of total splenic volume in mice [124] or as fraction of the total volume of the GC in rat [125], which may be used as GC cell count substitutes. These volumes showed a peak during the first phase of the GC. Such measurements have been used previously to validate a GC model [105]. However, other studies showed that there might not exist a typical GC in terms of size [126] and that GCs in a single immune response might not be synchronized [98]. The lack of precise quantitative data, current uncertainties in GC dynamics, and our decision not the model GC termination limits the possibilities and value of a compute-intensive parameter inference strategy to obtain values for the aforementioned parameters. However, instead of our trial-and-error approach, Approximate Bayesian Computation algorithms [127], MEANS [128], or other methods may be used to fit parameters on complex stochastic models such as ours.

Identification of expanded subclones

To determine a threshold that identifies expanded subclones we follow an approach that is similar to the method applied in our previous repertoire sequencing studies, e.g., [93, 101]. First, a histogram of counts c (cell counts for simulated data and read counts for experimental data) for all (un)expanded subclones is constructed to reflect their cell/read count frequencies $F(c)$ (Supplementary Figure S2). In general, subclones with low counts (e.g., $c = 1$) occur much more frequently (high F) than subclones with high count (e.g., $c = 100$). Next we define T as lowest count c for which $F(c) = 0$. That is, no subclones with c cells/reads are observed. We assume that $F(c \geq T) = 0$ for the un-

Table 1. Model parameters

B cell type	Proliferation rate (day^{-1})	Differentiation rate (day^{-1})	Apoptosis rate (day^{-1})
Centroblast (CB)	$\rho_{CB} = 4$ [129, 124, 130]	$\eta_{CB \rightarrow CC} = 6$ [91]	
Centrocyte (CC)		$\eta_{CC \rightarrow M} = 1$ [131] $\eta_{CC \rightarrow P} = 0.1$ [131] $\eta_{CC \rightarrow CB} = 1$ [91]	$\mu_{CC} = 4$ [102]
Plasma cell (P)			$\mu_P = 0.25$ [131]
Memory cell (M)			$\mu_M = 0.01$ [131]
Other parameters			
Capacity $A = 8000$		$k = 0.06, n = 1$ (S_d)	$s = 3.0$
Number of founder cells: 3		$k = 0.1, n = 4$ (S_a)	$r = 0.3$
Initial affinities: 0.1, 0.3, 0.5 mol^{-l}		$h = 20$	affinity shift = 0.1

derlying but unknown null distribution of unexpanded subclones. We define subclones with $c > T$ ($F(c) \geq 1$) to be expanded. That is, subclones observed with cell/read counts $c > T$ are larger than expected based on the distribution of unexpanded subclones. The threshold T is stringent but could be relaxed by defining the threshold T as the lowest count c for which $F(T) < p$, with $p \geq 1$.

The expansion threshold T was estimated for each individual simulation. We assumed that repertoire sequencing experiments measure mainly CCs since CBs do not, or at very low levels, express BCRs. Consequently, for the simulated data we determine threshold T from CC cell counts only. CC cell counts were taken from the last time point of the simulation.

Comparison of simulated and experimental data

We qualitatively compare subclone cell counts from our simulations to read counts from a single sample repertoire sequencing experiment. Since our computational model does not explicitly represent the BCR as a nucleotide (or protein) sequence we do not consider multiple (back) mutations occurring at previously mutated positions. Consequently, the number of different mutations and, hence, subclones in our simulation is slightly overestimated.

Each unique nucleotide read obtained from repertoire sequencing (RNAseq) can be considered as a unique subclone representing a set of mutations acquired during affinity maturation. Statistics calculated for these subclones can be compared to statistics calculated for the nucleotide-level subclones generated in our simulations. Alternatively, we can define subclones measured in the sample at the peptide level as having unique combination of V and J segments (determined by alignment) together with a unique CDR3. The peptide level definition allows to compare the statistics from the experimental data to the peptide-level simulations (include all three CDRs). In contrast to subclones analyzed at the nucleotide-level, this definition considers any mutations in the CDR3 for the

Table 2. Selected B-cell subclones from sample LN25

Subclone	Total		Largest cluster (lineage)	
	Subclones	Reads	Subclones	Reads
V3.7 - J4 (nt)	171	334	84	232
V3.74 - J4 (nt)	125	249	23	56
V3.23 - J4 (nt)	37	60	5	12
Total (nt)	333	643	112	300
V3.7 - J4 (pep)	89	606	19	36
V3.74 - J4 (pep)	97	519	9	14
V3.23 - J4 (pep)	76	193	7	12
Total (pep)	262	1318	35	62
			Second largest cluster (lineage)	
V3.7 - J4 (pep)	89	606	9	417

V and *J* nomenclature following IMGT [118, 107]. Subclones are defined as unique nucleotide sequences (nt) or as peptides (pep) with unique *V* and *J* assignment and a unique CDR3 sequence. For each *V*-*J* family the number of subclones and corresponding number of sequence reads are shown. The selected clusters for the given *V*-*J* segments correspond to the largest cluster of subclones having ≤ 2 differences at nucleotide or peptide level. For V3.7-J4 the second largest cluster, which contains the most abundant subclone, is also included.

experimental data, and affinity changing mutations in CDR1,2,3 for the simulated data.

Repertoire sequencing experiments performed on tissue (e.g., lymph node) generally results in a representation of subclones from multiple GCs and, most likely, different Ag responses, while in our simulation we generate subclones from a single GCR initiated by three founder clones. We account for this by selecting subclones corresponding to three lineages from sample LN25. We first map all reads against reference sequences extracted from the IMGT database to determine their *V* and *J* segments. Subsequently, observed combinations of *V* and *J* are counted, and reads corresponding to the three most abundant *V*-*J* combinations (V3.7-J4, V3.74-J4, V3.23-J4) are selected. The resulting three groups of reads still comprise subclones from multiple lineages. Therefore, we subsequently aligned all pairs of reads within each *V*-*J* group to determine the number of nucleotide differences (mutations) between them. Each pair of reads with two or fewer differences are connected to form clusters of subclones that are assumed to belong to the same lineage. Finally, the largest cluster (lineage) for each *V*-*J* combination was selected. The same procedure was followed at the peptide level. Since these three clusters did not include the most abundant subclone we also selected the second largest cluster from the V3.7-J4 subclones. The results of this procedure are shown in Table 4.2. Note that the number of differences between pairs of not connected reads within a cluster (lineage) may be larger than 2. These clusters of reads could in principle be subjected to further phylogenetic analysis to determine a lineage tree establishing their relationships [132]

4.3. Results

First we confirm that the computational model produces the dynamics of a typical GC response. We performed 15 repeated simulations with subclones defined at the nucleotide level. In agreement with previous work the GC response peaks around day 8 (Figure 4.5A) [124, 125, 126]. The size of the GC reaches approximately 14,000 cells, which is in agreement with estimations from histological sections of two GCs [133]. The CB to CC ratio (not shown) after day 8 remains between 1.4 and 2.0 is in agreement with data obtained from intravital microscopy [134]. The maximum number of SHMs in subclones emerging from our simulation ranges from 4 (day 10) to 11 (day 21) and is in good agreement with the 9 somatic mutations found in a single Ab after affinity maturation [135], with the 8 to 18 mutations found in an analysis of BCR sequences obtained from cells from GC sections derived from human lymph nodes [133], and with the 4 to 9 mutations observed in B cells from single GCs obtained from mice lymph nodes [136]. Monoclonal expansion of the 3 founder cells results in many low affinity subclones at the initial GC stage, but gradually higher affinity clones start to appear and out-compete lower affinity subclones. As expected from affinity maturation, and in agreement with other computational models (e.g., [102, 105]), the subclone population evolves to higher affinities (Figure 4.5B). The drop in the CB cell count after day 4 is caused by the initiation of SHM and the subsequent differentiation to CCs that may go into apoptosis. Since we do not model GC shutdown the cell counts remain relatively stable after 14 days. These results show that our computational model adequately captures the dynamics of a typical GCR.

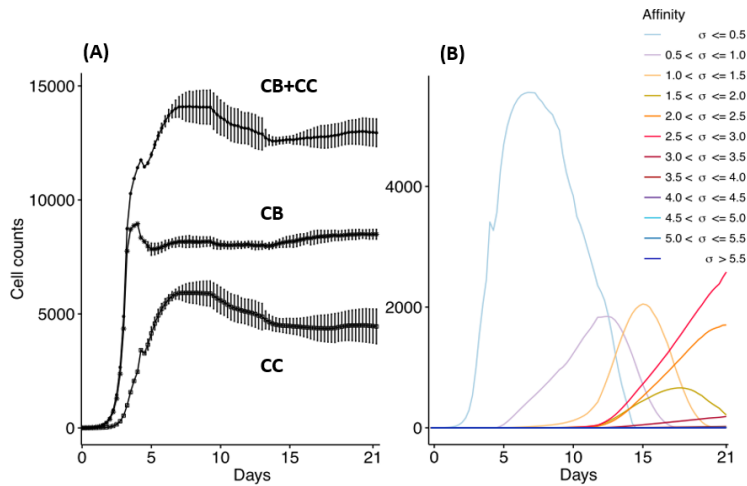


Figure 4.5: Overall GC dynamics emerging from the model. CB and CC with cell counts > 0 are plotted. (A) Dynamics of CB and CC cell counts during the GCR. Top curve shows the total cell count. Each point represents the average cell count of 15 simulations at time intervals of 6 hours (1 CB division). The vertical lines denote the standard deviations. (B) Evolution of absolute affinities during the GCR. Each colored line corresponds to an affinity class for which we summed the cell counts of the corresponding subclones.

Subclonal diversity

Figure 4.6 shows the dynamics of individual subclones during the GCR at the nucleotide and peptide level. Initially, 3 founder clones expand monotonically until day 4 after which SHM is initiated and new subclones with higher affinity start to be produced. The three low-affinity founder subclones reach high cell counts since, during monoclonal expansion, no lethal SHM occurs and $S_{\{d,a\}}$ assumes a large value (0.9) resulting in a very low rate of CB differentiation and CC apoptosis. New (higher affinity) subclones realize much lower cell counts because they start as single proliferating cells but are also reduced in count due to new mutation events and apoptosis as a result of competition with higher affinity subclones. Interestingly, although the population of subclones evolves to higher affinities (Figure 4.5B) there is not a single nor a small set of subclones that dominates this population during the later stages of the GCR. In fact, the number of unique subclones (Figure 4.6A) remains around 550 during the second half of the GCR.

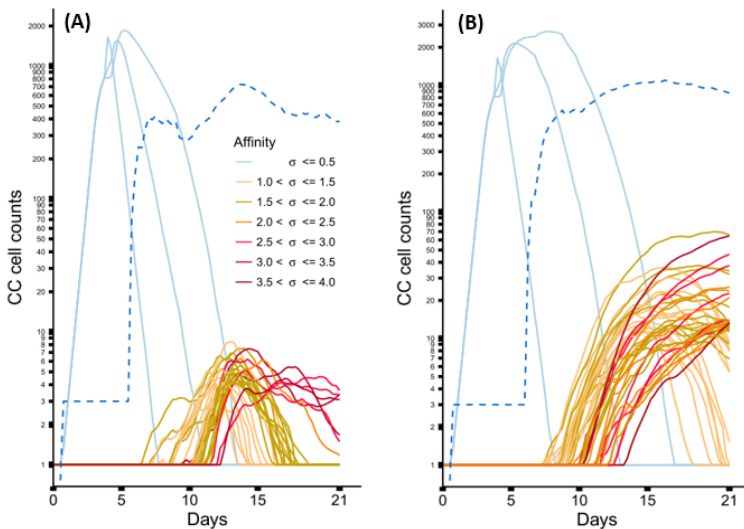


Figure 4.6: Dynamics of individual subclones from a representative simulations. (A) subclones defined at the nucleotide level. (B) subclones defined at the peptide level. Only subclones with (A) CCs cell counts ≥ 4 and (B) CCs cell counts ≥ 11 at any timepoint are shown. During the course of the GCR new subclones of higher affinity emerge (indicated by the colouring scheme). The light blue lines represent the 3 founder subclones of low affinity. The dotted blue line shows the number of unique subclones.

From sample LN25 we identified 112 nucleotide-level defined subclones (i.e. unique sequence reads) corresponding to 300 reads in the three largest lineages (Table 4.2). Since multiple sequence reads may originate from a single B-cell it is not possible to scale these numbers to 14,000 GC cells but obviously 300 reads do not represent this many GC cells. Therefore, these 112 subclones are an underestimation of the true number of subclones in a single GC. Although this number does not provide a validation for the 550 subclones observed in our simulations, it does show that the diversity of subclones in the experiment and the simulations is high. Using multiphoton microscopy and sequencing

it was recently shown that efficient affinity maturation can occur without homogenizing selection, and that loss of clonal diversity during the GCR varies widely from one GC to the other [136]. Note that when comparing Figure 4.6A (nucleotide level) to 4.6B (peptide level) the overall dynamic behavior is similar but the cell counts of higher affinity peptide-level subclones are about five times larger. An increase in cell count is expected since, in this scenario, neutral and synonymous somatic mutations do not result in new subclones and, hence, no reduction of cell counts. The number of unique subclones is still in the same order of magnitude as the previous simulation but counterintuitively increased compared to previous situation since a decrease is expected due to the fewer mutations imposed on these subclones. The observed increase is, however, a result of plotting and summing only the subclones with CC cell counts ≥ 1 . Including cell counts < 1 shows that the number of subclones does indeed decrease (data not shown).

Subclonal expansion

Expanded subclones are derived from experimental data on the basis of their peptide-level definition and relative abundance. Basically, this definition neglects any mutation in the V and J region as well as synonymous mutations in the CDR3. We identified expanded subclones from the experimental data (Figure 4.7). First, the expansion threshold was determined using all subclones from the LN25 sample resulting in 34 expanded subclones. Using this threshold ($T = 14$), a total of 3 and 9 subclones from the V3.7-J4 and V3.23-J4 subclones respectively are expanded. For each V-J family, Figure 4.7 also shows the subclones corresponding to the largest cluster (read counts ranging from 1 to 11), and for V3.7-J4, the subclones corresponding to the second largest cluster (read counts ranging from 1 to 261). This shows that subclones within a B-cell lineage may exhibit a wide range of read counts, which is in agreement with our simulated data. It also shows that the most abundant subclones do not necessarily belong to the largest cluster within a V-J family.

The clonal size (number of reads of a subclone divided by total number of reads) of the expanded LN25 subclones varies from 0.2 to 3.4%. Together, these represent 0.8% (34 out of 4454) of all subclones. This is similar to the amount of expansion found in one of our previous studies where clonal sizes $\geq 0.5\%$ were found to represent expanded subclones representing 0.3% and 1.9% of the subclones in peripheral blood and synovial tissue of RA patients respectively [101]. Since our computational model does not explicitly consider V and J segments, and because we cannot distinguish CDR3 from CDR1 and CDR2 mutations, we cannot group subclones resulting from our simulation in a way similar to the experimental data. However, by neglecting neutral and silent FWR/CDR mutations we can simulate subclones at the peptide level. The resulting subclones differ only in their CDR regions. The expanded peptide-level subclones in our simulation represent clonal sizes ranging from 0.3 to 8.7% representing 0.3 to 1.0% of the subclones. This degree of expansion is in the same order of magnitude as expansion observed in our experimental data.

BCR affinity of (un)expanded subclones

Repertoire sequencing only provides information about the relative abundance of B-cell subclones in a sample. In contrast, our computational model also provides information

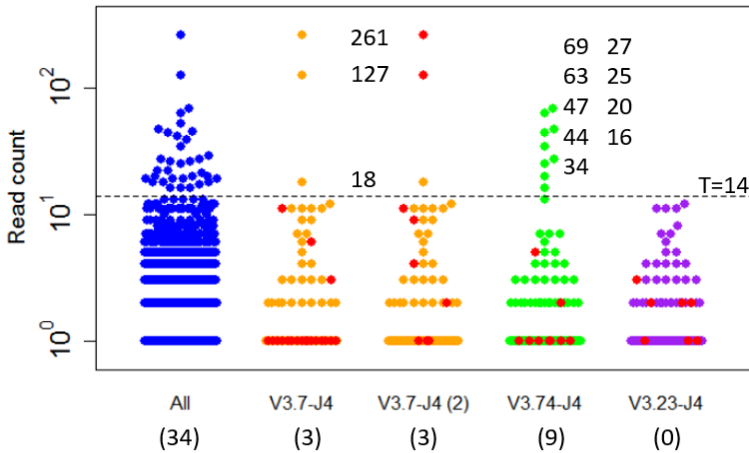


Figure 4.7: Subclones measured in a lymph node sample (LN25) from a healthy individual. The blue points show the read counts for all 4454 subclones measured in this sample (34 expanded subclones). The expansion threshold ($T = 14$) is determined from the all LN25 subclones, and indicated by the dashed line. Subclones of the three most abundant V-J combinations are shown in orange, green, and purple. The red dots indicate the subclones of the largest clusters and, for V3.7-J4, also the second largest cluster. Read counts of the expanded subclones are shown. The numbers in the parenthesis show the number of expanded subclones in the presented V-J subsets.

about the (relative) affinity of each subclone, which we use to gain insight in the affinity distributions among expanded and unexpanded subclones. High absolute affinity was defined by setting a threshold at the 75th percentile of absolute affinities of all subclones produced during the course of the GCR (range 1.53 – 10.6; 75th percentile is 3.00). Figure 4.8 shows the number of high and low affinity subclones among (un)expanded subclones for 15 simulations with subclones defined at the peptide level. The number of low affinity subclones among expanded cells varies from 17 to 70%, while the number of high affinity subclones among the unexpanded cells is relatively constant at about 25%. In 14 out of 15 simulations the affinity of most abundant subclones belongs to the highest 25% of affinities (Figure 4.9A) but these subclones never assume the highest affinity (Figure 4.9B). Figure 4.9B shows that the affinity tends to increase with subclone abundance (spearman rank correlation is 0.6) but that the largest affinities correspond to low abundant subclones. Increasing the affinity threshold to 95% results in more low affinity subclones among the expanded subclones (data not shown).

Although the affinity distributions depends on the expansion and affinity thresholds, the results demonstrate that lower affinity cells will be among the expanded subclones and *vice versa*. However, in a repertoire sequencing experiment one might not detect the very low abundant (high affinity) subclones. The high-affinity cells in the unexpanded fraction are either new subclones that have undergone significant affinity improvement but did not yet have sufficient time to proliferate, or are high-affinity subclones previously expanded but now being outcompeted by new subclones.

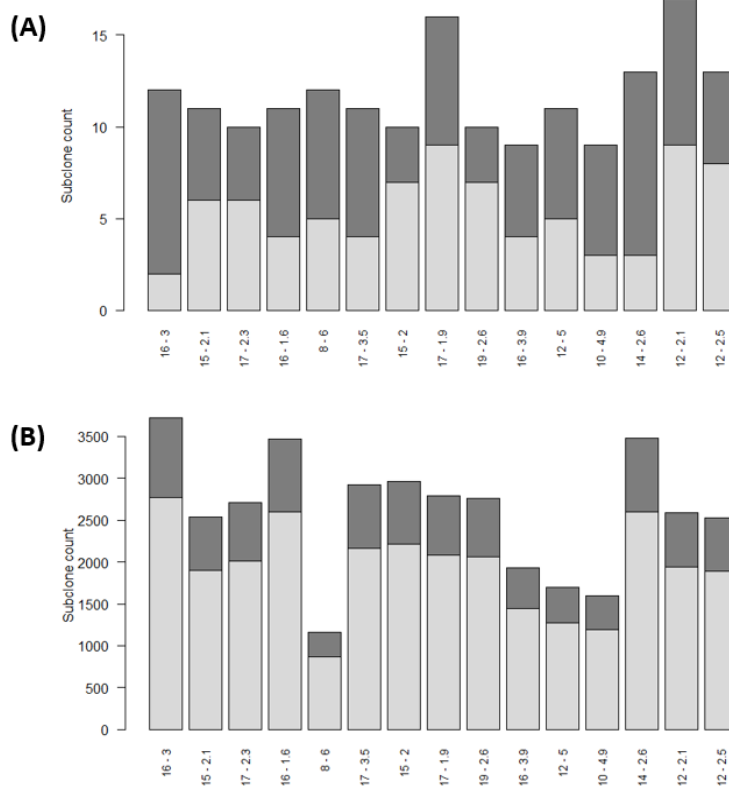


Figure 4.8: Numbers of high (dark gray) and low (light gray) affinity subclones among expanded (A) and unexpanded (B) subclones in 15 simulations (x-axis). Subclones were defined at the peptide level. There are many more unexpanded subclones compared to expanded subclones. Only subclones with CC cell counts > 0 were counts. The numbers at the x-axis denote the thresholds for expansion (T) and absolute affinity (75th percentile).

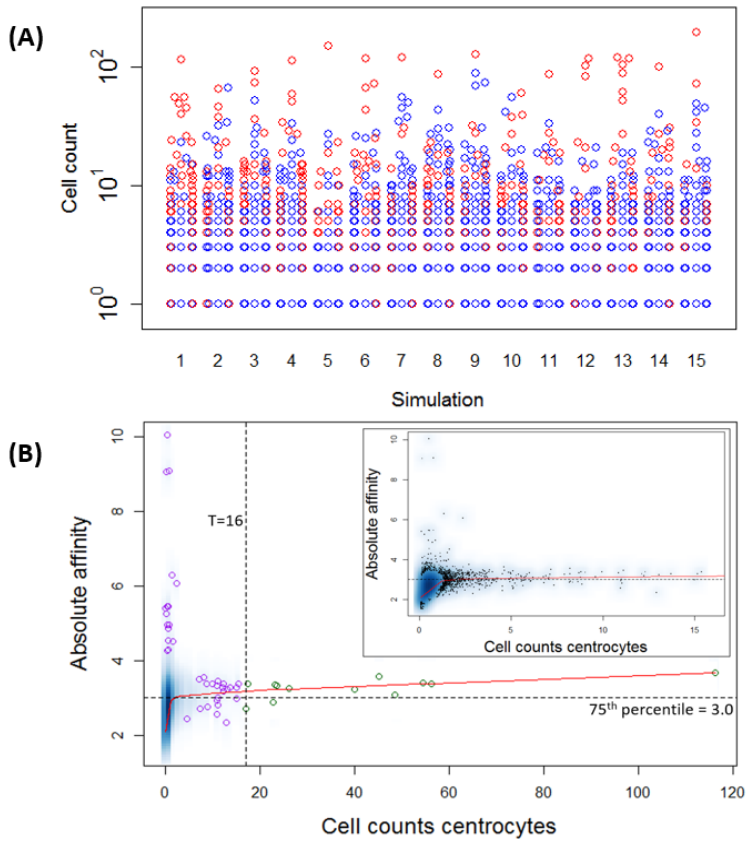


Figure 4.9: (A) distribution of high affinity subclones (red) among all subclones for 15 simulations. (B) Density plot of CC cell counts and absolute affinity for simulation 1. Inset shows only the low abundant subclones. Data points show a selection of subclones imposed on the density plot. Green points denote the expanded subclones. Purple points indicate a selection of low abundant subclones. The red line shows a lowess regression to indicate the overall relation between abundance and affinity.

4.4. Discussion

The identification of autoreactive B cells is important for understanding the pathogenesis of auto-immune diseases and developing therapies that target specific B cells to improve clinical outcome. However, for many autoimmune disorders the Ags are unknown which makes screening approaches challenging. Repertoire sequencing strategies have been developed as an alternative Ag-agnostic approach to identify autoreactive B cells relying on the assumption that expanded B cells measured in blood or tissue are involved in the pathogenesis of the disease. B-cell subclones identified by sequencing can be cloned and functionally characterized, and used to identify the autoantigen. In previous work we demonstrated that expanded clones identified by repertoire sequencing of synovium samples from RA patients point to putative autoreactive B cells [101]. This potentially provides the opportunity to develop novel therapeutic approaches targeting these cells.

(Deep) repertoire sequencing is successfully used for the identification of (autoreactive) B cells involved in immune disorders by relying on the assumption that expanded clones play a key role in the pathogenesis of the disease. However, no information is provided about the affinity of subclones measured with repertoire sequencing. It is reasonable to assume that expanded B cells have higher affinities than the background population of naive B-cells. However, since it is virtually impossible to measure affinity for many subclones detected in a sample, we developed a computational model to investigate the relation between subclone abundance and affinity. Although our computational model was not expected to provide precise quantitative results, we showed that the fraction of low affinity cells among expanded subclones, and the fraction of high affinity subclones among unexpanded B cells are substantial (Figure 4.8). Nevertheless, we showed a moderate positive correlation between subclone abundance and affinity. However, we also showed that the highest affinity subclones are of very low abundance. (Figure 4.9). We showed that the abundance of subclones within a lineage may vary widely. We conclude that repertoire sequencing is able to identify expanded Ag experienced clones but the most abundant subclones within these expanded clonal families are not necessarily the subclones with the highest affinity.

The abundancy-based selection of subclones is not a bad strategy since it leads to the identification of specific (sub)clones involved in (auto)immune disorders. The identified high abundant subclone can subsequently be characterized or used in Ag screening. Using the identified subclone together with phylogenetic analysis one could identify other subclone members of the same lineage and, subsequently, determine their affinities. The combination of abundancy and affinity might further guide the selection process. However, as explained, this is not feasible with current experimental approaches. There are, however, alternative selection strategies that can be used. For example, it has been shown that representative Abs selected from clonal families reconstructed by phylogenetic analysis neutralize influenza more effectively than “singleton” Abs that use heavy-chain V(D)J and/or light-chain VJ gene segments that are not used in any other Ab in the repertoire [95]. They showed that Abs from clonal families had significantly higher affinity than did singleton antibodies. Such strategy could be combined with subclone abundance. In previous work we have shown that the identification of pathogenic subclones in RA benefits from the selection of high-abundant subclones that are present in multi-

ple joints within a patient [101, 137]. It would be interesting to determine the affinity of these overlapping subclones in comparison to high abundant non-overlapping clones.

Our modelling efforts were motivated by the fact that it is currently infeasible to measure the affinities of large populations of subclones. We realize that at the same time this also prohibits direct experimental validation of the affinity distribution generated by our simulations. However, with evolving experimental technologies and approaches this may become feasible in the future. Using a tractable immunization mouse model and a well-defined Ag might be a first step towards validation. In this case a single cell strategy is required to sequence both the heavy and light Ig chains. Subsequently, the Igs must be cloned and expressed followed by measuring antibody-antigen binding kinetics using surface plasmon resonance [138]. However, it will remain difficult for clinical samples.

Surprisingly, our model shows that the number of unique subclones in a single GC remains remarkably constant throughout the GCR and does not evolve to a single or few high affinity dominating subclones although the affinity of the population as a whole increases as has been shown in previous studies [102, 105]. Moreover, the cell counts of individual subclones remain very low. Adding additional mechanistic detail (e.g., GC shutdown) is unlikely to change this observation. Moreover, this observation is in agreement with repertoire sequencing data and also seems in agreement with a recent study that showed that many clones may mature in parallel and sporadic clonal bursts generates many SHM variants of a clone [136].

Our model can be improved in several ways. Given the current results it would be interesting to investigate if our results would hold with more detailed GC models since with the model it is very difficult to control the amount of expansion by change the sigmoid functions without distorting the overall GC dynamics (although this might happen also *in vivo*). It would be interesting to investigate what exactly controls selection pressures and how this affects subclonal expansion and the BCR affinity distribution. Nevertheless, as we have shown, the current magnitude of expansion observed from the model is in the same order of magnitude as observed in experimental data. To allow a better comparison to the experimental data we plan to include an explicit representation of the BCR as a nucleotide sequence in our future model. This would allow to distinguish between the different CDR regions, to account for multiple (back) mutations at identical positions, and to more precisely specify subclones at both the nucleotide and protein level. In analogy to [139, 97], this would allow to explore the clonal composition and subclonal dynamics in a system where the best affinity BCR sequence is known and may be reached in few (key) mutations such as in the response against (4-hydroxy-3-nitrophenyl)acetyl [139, 97]. However, in general, the incorporation of realistic affinities in GC models will remain a challenge. Another interesting extension would include the egress of B cells to investigate the (sub)clonal composition in blood and to compare this to repertoire sequencing data obtained from blood samples.

Conflict of Interest Statement

The authors declare that the research was conducted in the absence of any commercial or financial relationships that could be construed as a potential conflict of interest.

Author Contributions

NdV and AvK designed the study. PR, AvK, JG, and PK defined the model. PR performed the simulations. PR and AvK analyzed the results from the simulations. PPT developed the protocol for acquiring LN samples, and provided the sample used in this study. RE conducted the repertoire sequencing experiment. PK, MD, BvS, AvK and NdV analyzed the experimental data. PR and AvK wrote the manuscript. All authors critically read, contributed, and approved the manuscript.

Funding

This work was carried out on the Dutch national e-infrastructure of SURFsara with the support of SURF Foundation. Research was supported by the Netherlands Bioinformatics Center (NBIC).

Acknowledgments

Prof. dr. Age Smilde (Biosystems Data Analysis Group) is acknowledged for critically reading and improving the manuscript. Dr. Huub Hoefsloot and Dr. Johan Westerhuis (Biosystems Data Analysis Group) are acknowledged for their suggestions during this research.

4.5. Supplementary Material

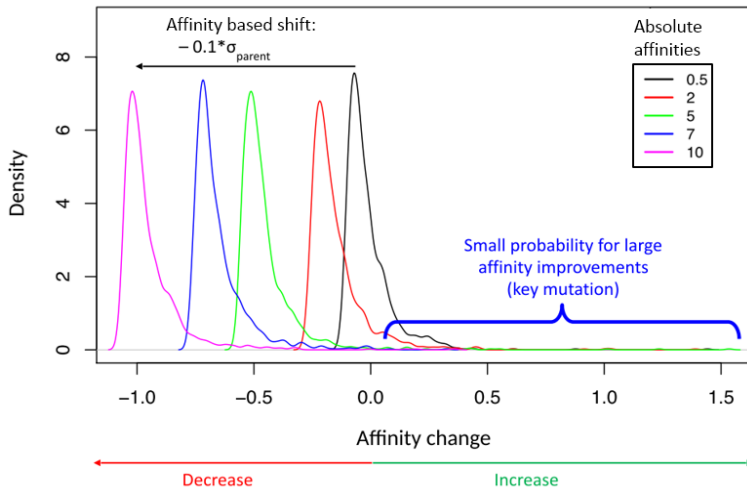


Figure 4.10: Distribution $f(\sigma)$ used to change affinity of mutated subclones. A mutation may decrease or increase the affinity of a B-cell. There is a small chance of making a large affinity improvements (representing key mutations). The distribution is shifted to the left with $0.1 * \sigma_{parent}$ for cells with higher affinities to decrease the chance for further improvements.

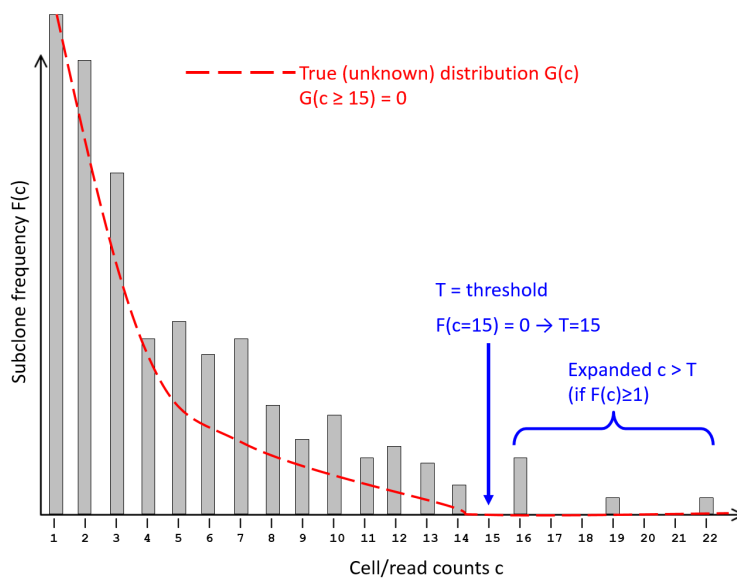


Figure 4.11: Determination of threshold for expanded subclones. See main text for further explanation.